Metabolism

Molecular Cancer Research

Real-Time Transferrin-Based PET Detects MYC-Positive Prostate Cancer

Rahul Aggarwal[1,2], Spencer C. Behr[3], Pamela L. Paris[2], Charles Truillet[3], Matthew F.L. Parker[3], Loc T. Huynh[3], Junnian Wei[3], Byron Hann[2], Jack Youngren[1], Jiaoti Huang[4], Gayatri Premasekharan[2], Nimna Ranatunga[2], Emily Chang[1], Kenneth T. Gao[3], Charles J. Ryan[1,2], Eric J. Small[1,2], and Michael J. Evans[2,3,5]

Abstract

Noninvasive biomarkers that detect the activity of important oncogenic drivers could significantly improve cancer diagnosis and management of treatment. The goal of this study was to determine whether ^{68}Ga-citrate (which avidly binds to circulating transferrin) can detect MYC-positive prostate cancer tumors, as the transferrin receptor is a direct MYC target gene. PET imaging paired with ^{68}Ga-citrate and molecular analysis of preclinical models, human cell-free DNA (cfDNA), and clinical biopsies were conducted to determine whether ^{68}Ga-citrate can detect MYC-positive prostate cancer. Importantly, ^{68}Ga-citrate detected human prostate cancer models in a MYC-dependent fashion. In patients with castration-resistant prostate cancer, analysis of cfDNA revealed that all patients with ^{68}Ga-citrate avid tumors had a gain of at least one *MYC* copy number. Moreover, biopsy of two PET avid metastases showed molecular or histologic features characteristic of MYC hyperactivity. These data demonstrate that ^{68}Ga-citrate targets prostate cancer tumors with MYC hyperactivity. A larger prospective study is ongoing to demonstrate the specificity of ^{68}Ga-citrate for tumors with hyperactive MYC.

Implications: Noninvasive measurement of MYC activity with quantitative imaging modalities could substantially increase our understanding of the role of MYC signaling in clinical settings for which invasive techniques are challenging to implement or do not characterize the biology of all tumors in a patient. Moreover, measuring MYC activity noninvasively opens the opportunity to study changes in MYC signaling in patients under targeted therapeutic conditions thought to indirectly inhibit MYC. *Mol Cancer Res; 15(9); 1221–9. ©2017 AACR.*

Introduction

The *MYC* oncogene is an important mediator of tumor initiation and progression in prostate cancer (1–3). In patients with metastatic castration-resistant prostate cancer (mCRPC), recent data implicate *MYC* (and closely related oncogene *MYCN*) in the emergence of treatment-associated small cell/neuroendocrine prostate cancer (tSCNC). tSCNC is a lethal disease subset that is increasing in prevalence in response to androgen ablation therapy (4, 5). Preclinical studies with prostate cancer models demonstrating that MYC hyperactivation in concert with PI3K/Akt/mTOR signaling can drive neuroendocrine differentiation and visceral metastasis formation provide support for a potential causal role of MYC in promoting tumor progression to an aggressive mCRPC phenotype (6).

MYC was previously thought to be "undruggable"; however, multiple classes of therapies are now aimed at indirectly inhibiting MYC or its downstream mediators. Foremost among them are bromodomain extra terminal (BET) inhibitors, which have demonstrated the ability to directly downregulate MYC expression. These inhibitors also display significant antitumor activity in a variety of androgen-independent, MYC-high prostate cancer cell lines and xenograft models (7–9). Multiple early-phase clinical trials of BET inhibitors in abiraterone/enzalutamide–resistant mCRPC are under way (e.g., NCT02705469, NCT02607228). Additional drugs targeting effectors of MYC signaling, including cyclin-dependent kinase (CDK) and PIM kinases, are also in preclinical and clinical development in prostate cancer and other solid tumor malignancies (10, 11).

Similar to how ^{18}F-dihydrotestosterone (DHT) PET fostered the development of the androgen receptor (AR) antagonists enzalutamide and apalutamide (12, 13), the burgeoning number of therapies aimed at inhibiting MYC underscores the need to develop a companion imaging biomarker capable of monitoring MYC transcriptional activity in real time, both to identify treatment-naïve patients whose tumors harbor hyperactive MYC, and to enable longitudinal assessment of MYC pathway modulation and therapeutic response.

MYC transcribes the transferrin receptor (TFRC; ref. 14). TFRC-targeting radiolabeled analogues may therefore serve as a

[1]Department of Medicine, Division of Hematology/Oncology, University of California San Francisco, San Francisco, California. [2]Helen Diller Family Comprehensive Cancer Center, University of California San Francisco, San Francisco, California. [3]Department of Radiology and Biomedical Imaging, University of California San Francisco, San Francisco, California. [4]Department of Pathology, Duke University, Durham, North Carolina. [5]Department of Pharmaceutical Chemistry, University of California San Francisco, San Francisco, California.

Note: Supplementary data for this article are available at Molecular Cancer Research Online (http://mcr.aacrjournals.org/).

R. Aggarwal and S.C. Behr contributed equally to this article.

Corresponding Author: Michael J. Evans, University of California San Francisco, 185 Berry Street, Lobby 6 Suite 350, San Francisco, CA 94107. Phone: 415-353-3442; Fax: 415-353-4925; E-mail: Michael.Evans@ucsf.edu

doi: 10.1158/1541-7786.MCR-17-0196

noninvasive quantitative measurement of MYC transcriptional activity. Consistent with this hypothesis, we have previously shown that ^{89}Zr coupled to transferrin via the chelator desferrioxamine is retained in cancer models in a MYC-dependent fashion (15–18). The goal of this study was to determine whether ^{68}Ga-citrate, a human ready radiotracer that measures TFRC expression levels *in vivo* (19), could be used to detect MYC-positive prostate cancer models and metastases [^{89}Zr-transferrin (^{89}Zr-Tf) is not yet cleared for human use]. Building on a pilot clinical study in which we showed that ^{68}Ga-citrate is taken up in human prostate cancer metastases (20), we conducted the first preclinical tumor imaging studies with ^{68}Ga-citrate, as well as the first patient studies of ^{68}Ga-citrate PET imaging coupled with analysis of cell-free DNA (cfDNA) and paired metastatic tumor biopsies to investigate whether ^{68}Ga-citrate can detect CRPC with MYC hyperactivity and neuroendocrine differentiation.

Materials and Methods

General methods

PC3 and 22Rv1 cells were obtained from ATCC and subcultured according to the manufacturer's recommendations. (+)-JQ1 was a generous gift from Dr. James Bradner (Dana-Farber Cancer Institute, Boston, MA). iBET-151 was purchased from Selleckchem and used without further purification. Human holo-transferrin was purchased from Sigma Aldrich, and succinimidyl-DFO was obtained from Macrocyclics. Zirconium-89 was purchased from 3D Imaging, LLC. ^{68}Ga-citrate was produced by the cyclotron core at University of California, San Francisco (UCSF, San Francisco, CA) and administered in buffered PBS.

Radioiodination of transferrin and *in vitro* uptake assays

Iodination with iodine-125 was done in precoated iodination tubes (Pierce). Transferrin (100 mg) was dispersed in 200 μL of PBS solution and added to the precoated iodination tubes. In a separate Eppendorf, 1 μL of HCl (0.2 mol/L), 2.5 μL of phosphate buffer (0.5 mol/L, pH = 8), and 10 μL of potassium iodide solution (1 mg/mL) was prepared. Iodine-125 (3 mCi; Perkin Elmer) was added into the tubes, and the previous solution was then mixed in the iodination tubes. After 15 minutes of reaction at room temperature, the solution was purified via PD10 column preequilibrated with 20 mL of PBS solution. The purity was assessed via iTLC, and ^{125}I-Tf was always > 98% pure.

PC3 and 22Rv1 cells were counted and plated at fixed cell concentrations between treatment arms. Cells were treated with vehicle or the bromodomain inhibitors iBET-151 or JQ1 (1 μmol/L) for 48 hours, whereupon they were washed and incubated with 10 μCi ^{125}I-Tf for 30 minutes at 37°C. After washing twice with PBS, the cell-associated activity was harvested in 1 mol/L NaOH (aqueous). The cell-associated activity was expressed as the percentage of total activity to which the cells were exposed. This value was further normalized to cell number to correct for treatment-induced changes in cell viability.

In vitro studies of MYC expression

PC3 and 22Rv1 cells (4×10^5) were incubated with vehicle, (+)-JQ-1 (1 μmol/L), and IBET-151 (1 μmol/L) at 37°C for 48 hours. Cells were lysed, and the mRNA was extracted using the Quick-StartProtocol (Qiagen). The mRNA was converted to cDNA using High-Capacity cDNA Reverse Transcription Kit (Applied Biosystems). Real-time PCR analysis was performed using PikoReal 96 Real-Time PCR System. *MYC* and *GADPH* expression (serving as housekeeper gene) levels were probed using validated sequences, and the relative ratio of the expression of the two genes was measured.

Animal studies

All animal studies were conducted in compliance with the Institutional Animal Care and Use Committee at UCSF. ^{89}Zr-Tf was prepared as reported previously (16). Three- to 5-week-old male *nu/nu* mice and C57BL/6 mice were obtained from Charles River Laboratories. Nu/nu mice were inoculated with 1×10^7 22Rv1 or PC3 cells subcutaneously into one flank in a 1:1 mixture (v/v) of media and Matrigel (Corning). Tumors were palpable within 14 to 21 days after injection. The drugs were suspended in HPMT solution (0.5% w/v hydroxypropylmethylcellulose dissolved in water plus 0.2% v/v Tween 80). Tumor-bearing mice were treated once daily via oral gavage with iBET-151 (30 mg/kg/day), (+)-JQ1 (50 mg/kg, twice a day), and vehicle for 3 days prior to radiotracer injection. Drug treatment continued during the 48 hours that ^{89}Zr-Tf distributed in the body. C57BL/6 mice were treated with 50 μL of neat turpentine in the right hind limb and injected 24 hours later with ^{68}Ga-citrate.

Small-animal PET and biodistribution studies

Tumor-bearing mice ($n = 5$/treatment arm) received approximately 400 μCi of ^{89}Zr-Tf or ^{68}Ga-citrate in 100 μL volume intravenously using a custom mouse tail vein catheter with a 28-gauge needle and a 100 to 150 mm long polyethylene microtubing (0.28 mm inner diameter × 0.64 mm outer diameter, Scientific Commodities, Inc.). Approximately 32 μg of ^{89}Zr-Tf at a specific activity of 0.4 mCi/nmol was administered per mouse. The mice were imaged on a dedicated small-animal PET/CT scanner (Inveon, Siemens Healthcare). Mice were imaged at 4 or 48 hours postinjection. Animals were scanned for 20 to 40 minutes for PET, and the CT acquisition was for 10 minutes. The coregistration between PET and CT images was obtained using the rigid transformation matrix from the manufacturer-provided scanner calibration procedure, as the geometry between PET and CT remained constant for each of PET/CT scans using the combined PET/CT scanner. Animals were anesthetized with isoflurane gas at 2% concentration mixed with medical grade oxygen. PET data were framed dynamically for the first two time points. The durations of the 0.5-hour PET data were: 10 × 10 seconds, 5 × 40 seconds, 1 × 300 seconds, and 5 × 600 seconds. The 3- to 5-hour PET data were also divided to two 1,800-second frames. The *in vivo* CT parameters were 120 projections of continuous rotations to cover 220° with an X-ray tube operated at 80 kVp, 0.5 mA, and 175 ms exposure time.

Manufacturer-provided ordered subsets expectation maximization algorithm was used for PET reconstruction that resulted in 128 × 128 × 159 matrices with a voxel size of 0.776 × 0.776 × 0.796 mm^3. The CT image was created using a conebeam Feldkamp reconstruction algorithm (COBRA) provided by Exxim Computing Corporation. The matrix size of the reconstructed CT images was 512 × 512 × 662 with an isotropic voxel size of 0.191 × 0.191 × 0.191 mm^3. The photon attenuation correction was performed for PET reconstruction using the coregistered CT-based attenuation map to ensure the quantitative accuracy of the reconstructed PET data.

To evaluate the uptake of ^{68}Ga and ^{89}Zr-Tf radiotracers in human xenografts, biodistribution studies were conducted following imaging. Animals were euthanized by CO_2 asphyxiation after scans were completed. Blood, muscle, and tumor were harvested immediately following sacrifice. The tissues were weighed and counted using a Wizard3 gamma counter (PerkinElmer) to assess ^{68}Ga or ^{89}Zr concentration. Calibration with known amounts of ^{68}Ga and ^{89}Zr was performed to determine the amount of activity in each organ. This activity was then decay corrected, and the percentage of the injected dose per gram (%ID/g) of tissue was calculated and reported.

Patient selection and clinical study design

The clinical study was approved by the UCSF Institutional Review Board, and all patients provided written informed consent before study enrollment. All patients had histologically confirmed prostate cancer and had developed progressive metastatic castration-resistant disease by PCWG2 criteria. All had progressive disease following treatment with abiraterone and/or enzalutamide (21). Patients were required to undergo conventional scans including cross-sectional imaging of the chest/abdomen/pelvis and whole-body radionuclide bone scan (either ^{99m}Tc- HDP or ^{18}F-NaF) within 12 weeks prior to ^{68}Ga-citrate PET imaging. All included patients had imaging evidence of at least three metastatic lesions by conventional imaging. On the day of ^{68}Ga-citrate PET imaging, prior to tracer injection, patients had peripheral blood collected for determination of cell-free tumor DNA *MYC* copy number status. A subset of patients underwent CT-guided core needle biopsy of an accessible metastatic lesion performed within 4 weeks following completion of ^{68}Ga-citrate PET imaging. Patients underwent an optional second ^{68}Ga-transferrin PET scan within 12 weeks of the first scan.

PET imaging protocol

Patients were injected with up to 15 mCi [555 MBq; average 7.42 mCi (274.6 MBq), range 3.7–11.9 mCi (136.9–438.5 MBq)] ^{68}Ga-citrate intravenously. PET acquisition was acquired between 120 and 263 minutes after injection (average 210 minutes). Images were acquired on either a PET/CT or PET/MR. PET/CT examinations were performed on either a Biograph 16 (Hi-Rez) PET/CT scanner (Siemens AG) with an integrated PET and 16-MDCT scanner or a Discovery VCT PET/CT scanner (GE Medical Systems) with an integrated PET and 64-MDCT scanner. A low-dose CT was acquired for PET attenuation correction. PET/MR images were performed on a SIGNA PET/MR (GE Medical Systems). Attenuation correction for PET reconstruction was performed using an MR-based attenuation correction technique provided by the scanner manufacturer.

Image analysis

Maximum-intensity projection, axial, coronal, and sagittal reconstructions and PET/MR-fused images were reviewed on an Advantage Windows Workstation (AW). PET images were evaluated by trained nuclear medicine physician blinded to the results of conventional imaging scans as well as clinical/genomic features of the case and scored for the presence of PET avid lesions. Lesions were considered PET positive if uptake was focal, greater than the adjacent background soft tissue, and not in an expected physiologic structure, such as the urinary bladder, vessels, or salivary glands,

For semiquantitative analysis, a volume of interest was manually drawn around PET-avid lesions and SUV_{max} was recorded. The location of abnormal radiotracer uptake was compared with CT and nuclear medicine bone scans. In addition, SUV_{mean} values were recorded in the liver, paraspinous soft tissues, bone (right sacrum), and mediastinal blood pool for determination of normal structures.

With conventional imaging, soft tissue metastases were considered positive if greater than 1 cm in long axis, except for lymph nodes that were considered positive if greater than 1.5 cm in short axis. Bone lesions on radionuclide scan were considered positive if uptake was focal and not in a pattern consistent with arthritis or antecedent trauma/fracture.

cfDNA analysis of MYC amplification

Blood (20 mL) was collected from mCRPC patients in purple top EDTA tubes and was fixed using 10% neutral-buffered solution containing 4% paraformaldehyde within 2 hours of receiving the sample. Plasma was isolated immediately from the fixed blood by centrifuging the samples for 10 minutes at 200 × *g* at room temperature, followed by a second spin at 1,600 × *g* for 10 minutes. Avoiding the buffy coat, plasma was carefully transferred to new 15-mL tubes and centrifuged at 1,600 × *g* for an additional 10 minutes. The plasma was transferred to 50-mL tubes and stored at −80°C. cfDNA was extracted from plasma using the QIAamp Circulating Nucleic Acids Kit (Qiagen) according to the manufacturer's protocol. The extraction was carried out within a week of the plasma extraction. The extracted cfDNA was eluted in 20 μL of AE (Qiagen) buffer and assayed for *MYC* copy number using Digital PCR (QuantStudio, Life Technologies). 1× QuantStudio 3D Digital PCR Master Mix V2 (Applied Biosystems), TaqMan copy number assay Hs02045885_cn (*MYC*), and 1× RNAseP TaqMan copy number reference assay (Applied Biosystems) were used in the reaction. DNA extracted from PC3 cell lines and PC3 DNA spiked into healthy donor blood was used as positive (*MYC* amplified) controls, while male normal germline DNA was used as negative control (*MYC* wild type). Six microliters of cfDNA was combined with the PCR reaction mix and loaded onto a QuantStudio 3D Digital PCR 20K chip. The QuantStudio 3D Analysis Suite Software was used to evaluate *MYC* copy number for each patient sample based on the reference gene (RNAseP) copy number (i.e., two copies).

Analysis of histologic evidence of small-cell neuroendocrine carcinoma in metastatic tumor biopsies

FFPE tissue was histologically evaluated in a central CLIA-certified laboratory for evidence of neuroendocrine differentiation by morphologic and IHC criteria (22).

Statistical analysis

The percentage of injected activity taken up in prostate cancer tumors versus other organs in mice was injected with either ^{68}Ga-citrate or ^{89}Zr-Tf analyzed using the unpaired, two-tailed Student *t* test. Differences at the 99% confidence level ($P < 0.01$) were considered to be statistically significant. The imaging data from patient studies were summarized using descriptive statistics. Fisher exact test was used to compare frequency of PET-avid lesions across organ site.

Results

^{68}Ga-citrate shows MYC-dependent uptake in human prostate cancer models

^{68}Ga-citrate has not been previously evaluated in tumor-bearing mice. Therefore, we first conducted a time course study in *nu/nu* mice bearing subcutaneous PC3 xenografts, a MYC-positive model of human prostate cancer, to define the optimal time point postinjection to study ^{68}Ga-citrate. Mice received 400 to 500 μCi of ^{68}Ga-citrate, and biodistribution studies were conducted at 2, 4, and 6 hours postinjection (Fig. 1A; Supplementary Fig. S1). Peak tumor uptake was observed at 4 hours postinjection. Moreover, blood pool activity declined from 2 to 4 hours postinjection and remained stable from 4 to 6 hours postinjection. Radiotracer uptake in normal tissues (liver, spleen, kidney, and muscle) saturated within 2 hours postinjection, and the level of uptake was lower than what was observed in the tumor. The highest tumor-to-blood and tumor-to-muscle ratios were found to be at 4 and 6 hours postinjection (Supplementary Table S1). A follow-up study in mice bearing subcutaneous 22Rv1 xenografts, an AR, and MYC-positive model of human prostate cancer also showed high ^{68}Ga-citrate uptake 4 hours postinjection, with similar uptake in normal mouse tissues and compartments (Fig. 1B; Supplementary Fig. S2).

Because blood pool activity was approximately equivalent with tumor uptake of ^{68}Ga-citrate in both mouse cohorts, we next tested whether tumor uptake of ^{68}Ga-citrate was equivalent with that of ^{89}Zr-Tf at time points we previously showed to reflect receptor-mediated binding to tumors (15–17, 23, 24). We reasoned that equivalent levels of radiotracer uptake in tumor would be strong evidence of specific receptor binding by ^{68}Ga-citrate. *Nu/nu* mice bearing subcutaneous 22Rv1 xenografts were treated with approximately 400 μCi of ^{89}Zr-Tf, and radiotracer biodistribution was studied 48 hours postinjection. Blood pool–associated activity was significantly lower than that of tumor, as expected (Fig. 1C). Moreover, tumor uptake of ^{89}Zr-Tf was equivalent to the uptake of ^{68}Ga-citrate.

To further show evidence of specific receptor binding by ^{68}Ga-citrate at 4 hours postinjection, a cohort of *nu/nu* mice bearing subcutaneous PC3 or 22Rv1 tumors was pretreated with vehicle or the BET bromodomain inhibitors (+)-JQ1 or iBET-151. Both JQ1 and iBET-151 therapies downregulated MYC mRNA and Tf uptake *in vitro* (Supplementary Fig. S3). Tumors in the mice receiving 5 days of treatment had significantly less ^{68}Ga-citrate uptake (Fig. 2A and B; Supplementary Figs. S4 and S5). Moreover, the percent change in tumor uptake observed in BET inhibitor–treated mice was similar between ^{68}Ga-citrate and ^{89}Zr-Tf (^{89}Zr-Tf biodistribution was studied 48 hours postinjection).

^{68}Ga-citrate has been used in tumor-naïve humans and rodents to detect the focal accumulation of activated leukocytes due to inflammation or infection (25). On this basis, we tested whether ^{68}Ga-citrate could quantitatively distinguish tumor from an inflammatory abscess. A cohort of tumor-naïve mice was injected with approximately 50 μL of turpentine in the right hind limb to induce an acute phase response, and the mice were treated with ^{68}Ga-citrate 24 hours after injection. PET and biodistribution studies conducted 4 hours after radiotracer injection showed detectable accumulation of ^{68}Ga-citrate in the inflamed muscle above the contralateral untreated hind limb (Fig. 2C). The magnitude of ^{68}Ga-citrate accumulation in the inflamed muscle was statistically lower than what was observed in either prostate cancer tumor using the same imaging conditions.

Patient imaging results

Twenty patients were enrolled in the study between May 2015 and December 2016. Baseline characteristics are shown in Supplementary Table S2. All patients had mCRPC with prior progression on abiraterone and/or enzalutamide.

A total of 326 lesions were detected on conventional imaging (CT, ^{99m}Tc-HDP), of which 53% were avid for ^{68}Ga-citrate. Roughly two thirds (63.8%) of osseous lesions were avid for radiotracer, while approximately 20% of lymph node and approximately 5% of visceral organ lesions were avid. Significant qualitative and quantitative intertumoral heterogeneity was observed with respect to ^{68}Ga-citrate uptake (Fig. 3). A total of 174 metastatic lesions (53.3%) were PET avid and 152 (46.7%) were negative on ^{68}Ga-citrate PET imaging. The average SUV_{max} of ^{68}Ga-citrate–positive lesions was 5.74 (SD, 2.89; range, 1.8–19.4). The median percentage of PET-positive lesions per patient was 50% (range, 0%–93%). There was no relationship between dose of ^{68}Ga-citrate or tumor uptake time with the percentage of PET-avid lesions or intratumoral SUV_{max}. PET-avid lesions were

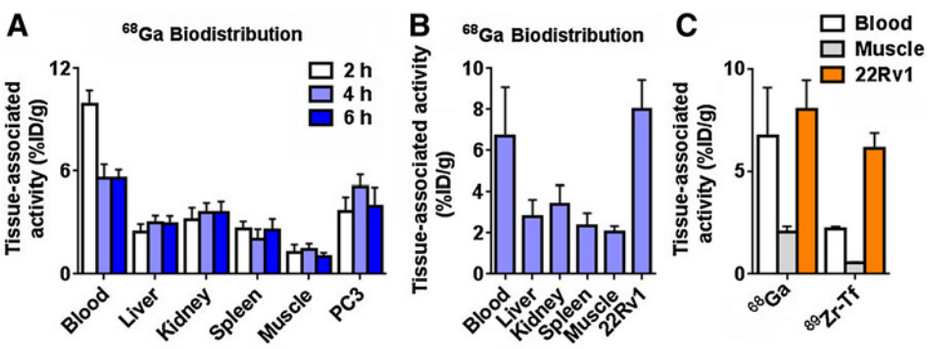

Figure 1.

A, A biodistribution study showing the accumulation of ^{68}Ga-citrate in normal mouse tissues and subcutaneous PC3 tumors at 2, 4, and 6 hours postinjection. Peak radiotracer uptake was observed in the tumors at 4 hours postinjection. **B,** A biodistribution study showing the relative distribution of ^{68}Ga-citrate in normal mouse tissues and subcutaneous 22Rv1 tumors at 4 hours postinjection. **C,** Biodistribution data from mice bearing subcutaneous 22Rv1 tumors showing that the amount of ^{89}Zr-Tf uptake in the tumors at 48 hours postinjection is equivalent to the amount of ^{68}Ga-citrate uptake in tumors at 4 hours postinjection. Importantly, the tumor uptake of ^{89}Zr-Tf exceeded blood pool activity, showing that approximately 7% ID/g is a value that can represent specific binding.

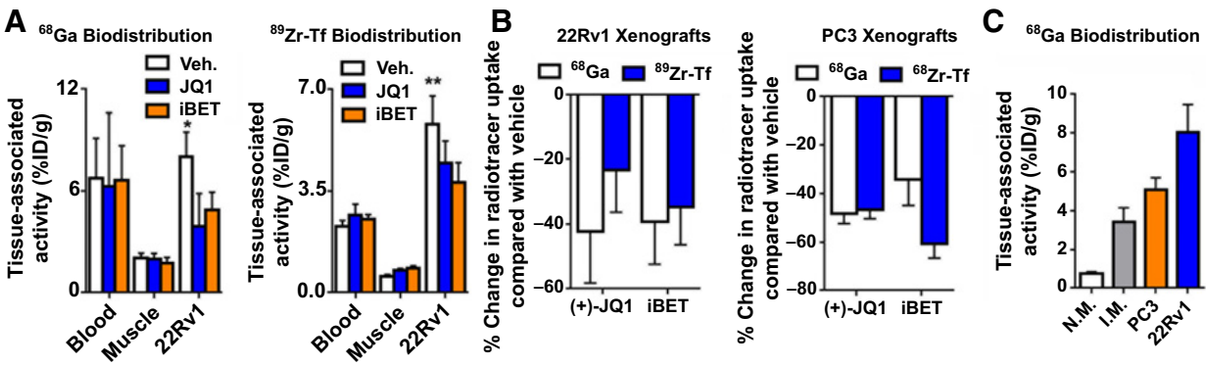

Figure 2.

A, Biodistribution data from nu/nu mice bearing subcutaneous 22Rv1 xenografts shows reduction of tumor uptake of ^{89}Zr-Tf and ^{68}Ga-citrate after treatment with (+)-JQ1 or iBET-151. Mice were treated for 5 days prior to radiotracer administration. Biodistribution studies were conducted 4 hours postinjection of ^{68}Ga-citrate, and 48 hours postinjection of ^{89}Zr-Tf. Drug treatment continued while ^{89}Zr-Tf equilibrated into peripheral tissues. *, $P < 0.01$; **, $P < 0.05$. **B,** A plot showing the equivalent percent reduction in tumor uptake of ^{68}Ga-citrate or ^{89}Zr-Tf due to MYC and TFRC suppression by (+)-JQ1 or iBET-151. **C,** A plot of biodistribution values for ^{68}Ga-citrate in normal muscle (N.M.), an inflamed muscle (I.M.) due to turpentine treatment, and the two prostate cancer tumors show that radiotracer uptake is higher in tumor.

more likely to be detected in the bone versus soft tissue (63.8% vs. 12.1%; $P < 0.0001$; Table 1). Figure 4 highlights a particular example of a patient with heterogeneous ^{68}Ga-citrate uptake within metastatic lesions in the bony pelvis, with adjacent lesions demonstrating widely varying degree of intratumoral uptake.

^{68}Ga-citrate PET uptake in tumor and normal organs is reproducible upon serial imaging

Four patients underwent paired imaging with ^{68}Ga-citrate PET imaging, with a median interval of 37 days (range, 30–39 days) between scans (Supplementary Table S3). During this interval, patients were clinically stable and had no significant change in serum PSA level to indicate disease progression. The average change in SUV_{mean} between patient scans for blood pool, liver, paraspinous muscles, and bones was 0.38 (range = −0.4–0.4; SD = 0.05), 0.25 (range = −0.6–0.1; SD = 0.24), 0.28 (range = −0.4–0.4; SD = 0.15), and 0.3 (range = −0.4–0.3; SD = 0.08). Across all PET-avid metastatic lesions for these 4 patients ($N = 10$; all osseous), there was likewise no significant difference in ^{68}Ga-citrate uptake between pre- to postscans [mean change from baseline in SUV_{max} = −0.29 (range −5.3–1.4; SD = 1.89).

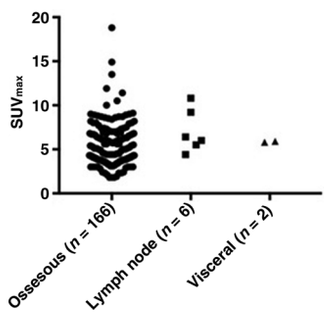

Figure 3.

Distribution of intratumoral ^{68}Ga-citrate PET uptake by site of metastasis in the patient cohort. SUV_{max} = maximum standardized uptake value on PET per lesion

Pronounced ^{68}Ga-citrate PET uptake is observed in a subset of mCRPC patients with high tumor *MYC* amplification

Eighteen of 20 patients (90%) were evaluable for *MYC* copy number gain by cfDNA analysis. We observed a gain of at least one copy of *MYC* in 16 of 18 (89%) evaluable samples (Table 2). This is generally consistent with prior reports demonstrating high prevalence of 8q chromosome gain in prostate cancer (26, 27). All 16 patients with evidence of *MYC* copy gain on cfDNA analysis had at least one ^{68}Ga-citrate–avid metastatic lesion. Higher level focal *MYC* amplification (>2 copy number gain) was observed in 6 patients (33%), also consistent with prior molecular analyses of mCRPC tumors. Although the limited sample size precludes definitive assessment of an association between *MYC* amplification in cfDNA with ^{68}Ga-citrate PET, the subset of 6 patients with high level *MYC* amplification on cfDNA demonstrated a higher percentage of ^{68}Ga-citrate–avid lesions compared with those without *MYC* amplification (68.8% vs. 46.6%). Figure 5 illustrates one such patient (patient-004) with MYC amplification on cfDNA analysis (estimated 6 copies of *MYC* gained) with striking PET avidity on ^{68}Ga-citrate PET, with 29 of 32 total osseous metastases (90%) positive for uptake (average SUV_{max} = 6.3/lesion).

^{68}Ga-citrate PET detects tumors with histologic and serologic evidence of neuroendocrine differentiation

Eleven patients (55%) underwent CT-guided metastatic tumor biopsy following ^{68}Ga-citrate PET scan. The median time interval between PET scan and subsequent image-guided tumor biopsy was 6 days (range, 4–38). Of the 7 patients with metastatic tissue evaluable for histologic analysis, one demonstrated pure SCNC differentiation on pathology review (patient-011), and the other six tumors demonstrated adenocarcinoma differentiation (Supplementary Table S4). The tumor with pure SCNC histology was located in the right femur of this patient (Fig. 6). On coupled ^{68}Ga-citrate PET imaging, this lesion demonstrated high avidity for the tracer, above the median for the patient cohort (SUV_{max} = 6.9) and significantly higher than adjacent metastatic lesions (Fig. 6). Genomic interrogation of the metastatic tumor biopsy

Table 1. Distribution of PET-avid metastatic lesions by body site

Organ site	Number of lesions on conventional imaging	Number of PET-avid lesions on ^{68}Ga-Tf PET (%)	Average SUV_{max} (SD)
Bone	260	166 (63.8%)	5.63 (2.76) Range, 1.8–18.8
Lymph node	29	6 (20.7%)	7.04 (2.43) Range, 4.4–10.8
Visceral organ	37	2 (5.4%)	5.85 (0.07) Range, 5.8–5.9

revealed high-level *MYC* amplification (estimated 4 copy number gain), consistent with prior reports of treatment-emergent SCNC. An additional patient (patient-004) had serologic evidence of neuroendocrine differentiation (serum chromogranin = 66 ng/mL; upper limit of normal = 15 ng/mL) with a concordant markedly positive PET scan with 29 of 32 metastatic lesions positive for uptake, as previously described above (Fig. 5).

In the 2 patients with genomically evaluable paired cfDNA and metastatic tumor biopsies, it is worth noting that patient-011 demonstrated only 1 copy gain of *MYC* in analysis of cfDNA versus 4 copies gained in metastatic biopsy. Patient-003, in contrast, demonstrated three copies of *MYC* gained in both metastatic biopsy and cfDNA. These results support the significant interlesional and interpatient heterogeneity observed on PET imaging and highlight the difference between lesion-specific genomic assessment and aggregated results on cfDNA analysis.

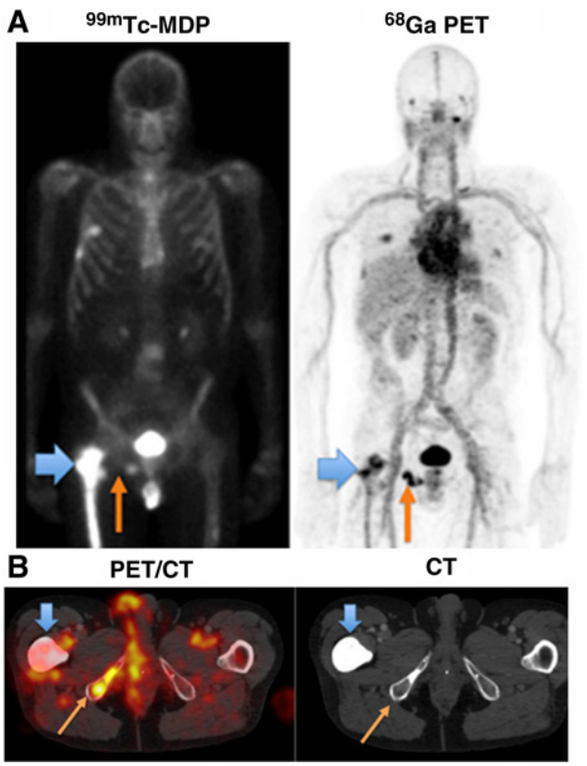

Figure 4.
^{68}Ga-citrate uptake is heterogeneous among lesions detected with conventional imaging in the same patient. **A,** Multiple regions of uptake on ^{99m}Tc-HDP bone scan (left) including intense uptake in the right femur (blue arrow). Although the ^{68}Ga-citrate PET MIP image (right) shows matching uptake in the right femur (blue arrow), it also reveals discordant uptake in the right ischium (orange arrow). **B,** Axial PET, CT, and fused ^{68}Ga-citrate PET/CT through the right ischium show that the CT is normal in region of ^{68}Ga-citrate uptake in the right ischium. CT also showing sclerosis in the region of the abnormal bone scan and ^{68}Ga-citrate uptake (blue arrow).

^{68}Ga-citrate uptake is recapitulated in the patient-derived xenograft of a liver metastasis

We isolated tumor tissue from the liver metastasis (patient-003) and propagated it in a NOD/SCID mouse model (Supplementary Fig. S7). The patient-derived xenograft (PDX) tumor was histologically similar to the tumor biopsy (Supplementary Fig. S8) and demonstrates similar mRNA transcript levels (log-scale) of *MYC* (liver metastasis = 10.9; PDX = 10.6) and *TFRC* (liver metastasis = 13.2; PDX = 12.3). Upon imaging of the PDX tumor with ^{68}Ga-citrate PET, we observed comparable intratumoral uptake as that observed in the liver metastasis from the patient PET scan (% ID/g = 2.3 ± 0.9 in PDX tumor; SUV_{mean} = 4.9 in liver metastasis, see Supplementary Fig. S9).

Discussion

In this report, we show that both human prostate cancer models and clinical disease bearing the molecular and/or histologic features of MYC hyperactivity are detectable with ^{68}Ga-citrate PET. Our preclinical experiments show specific tumor binding of ^{68}Ga-citrate in MYC-high prostate cancer cell lines and xenograft models and suggest a novel tool to permit functional read-out of pharmacologic inhibition of the MYC signaling pathway by BET inhibitors and perhaps other emerging therapies. In patients with mCRPC, we show that a subset of patients harbored markedly ^{68}Ga-citrate–avid tumors with concordant molecular evidence of MYC activation detectable in paired analysis of cfDNA. With biopsy, two examples are shown of patients with histologic or serologic evidence of SCNC, and they also have tumors markedly avid for ^{68}Ga-citrate. These results provide robust justification to further investigate the clinical application of ^{68}Ga-citrate PET as a real-time, noninvasive monitoring tool that can potentially capture MYC-driven prostate cancer, including tumors with SCNC histology.

MYC transcriptional activity is associated with SCNC, a subset of advanced prostate cancer that is highly lethal, and that can be difficult to identify without invasive and sometimes technically challenging metastatic biopsies. Although MYC inhibitors are under development, pharmacodynamic markers of MYC inhibition are not readily available. Therefore, these data are timely and significant, as the successful outcome of preclinical and/or clinical trials with indirect MYC inhibitors will likely depend on biomarkers like ^{68}Ga-citrate that can identify treatment-naïve tumors with MYC hyperactivity (which therefore may be most likely to respond to an anti-MYC inhibitor), as well as monitor the down-regulation of MYC activity longitudinally that might predict a clinical response to treatment.

Our preclinical experiments indicate a high degree of tumor specificity of ^{68}Ga-citrate for MYC-high prostate cancer cell lines and xenograft models and suggest a novel tool to permit functional read-out of pharmacologic inhibition of the MYC signaling

Table 2. *MYC* copy number status in cfDNA by digital PCR analysis

Samples	# of *MYC* copies gained	# of *MYC* copies gained, rounded
PC3 stock (+MYC) control	2.74	3
PC3 cfDNA (+MYC) control	1.58	2
Male germline DNA (WT MYC)	0	0
Patient-001	1.16	1
Patient-003	3.48	3
Patient-004	6.28	6
Patient-005	0.66	1
Patient-006	0.68	1
Patient-007	1.3	1
Patient-008	0.32	0
Patient-010	0.58	1
Patient-011	0.78	1
Patient-012	3.5	4
Patient-013	0.74	1
Patient-014	1.84	2
Patient-015	1.1	1
Patient-016	2.76	3
Patient-017	0.28	0
Patient-018	4.34	4
Patient-019	5.78	6
Patient-021	0.82	1

Figure 5.
A maximum-intensity projection (MIP) image of patient-004 demonstrating widespread uptake within multilevel osseous metastases within the spine, with concurrent cfDNA evidence of focal, high MYC copy gain.

pathway by BET inhibitors and perhaps other emerging therapies. In patients with mCRPC, we show that the subset of patients with focal *MYC* amplification detectable in cfDNA harbored a higher proportion of tumors with ^{68}Ga-citrate–avid avidity. We further demonstrate that ^{68}Ga-citrate PET intratumoral uptake is reproducible but with appreciable intertumoral and interpatient heterogeneity that may reflect divergent clonal evolution with varying degree of MYC hyperactivation in the treatment-resistant mCRPC setting (28). Whole-body ^{68}Ga-citrate PET imaging may therefore represent a valuable novel tool to annotate the degree of intertumoral heterogeneity with respect to MYC/neuroendocrine signaling in a noninvasive, real-time fashion.

The underlying reason for the preferential ^{68}Ga-citrate PET avidity in bone lesions relative to soft tissue metastases is not readily apparent. There are no significant differences in *TFRC* expression levels by anatomic site of disease in mCRPC in ours and other publicly available datasets. One prior report has suggested that ^{68}Ga-citrate accumulation is due to regional variation in perfusion and non–receptor-mediated accumulation in regions of leaky vasculature (27). The consistency in ^{68}Ga-citrate uptake between our PDX subcutaneous model and *in situ* liver metastasis, however, supports tumor-specific uptake as opposed to regional vascular permeability as the predominant determinant of radiotracer accumulation. Additional studies in CRPC patients harboring soft tissue metastases will be necessary to fully characterize the expected pattern of ^{68}Ga-citrate PET uptake in nonosseous sites of metastases.

Asangani and colleagues previously did not observe any downregulation of MYC in PC3 cells when treated with (+)-JQ1 (8). Reviewing each study carefully, we hypothesize that methodologic differences in the experiments may account for the apparent discrepancy with our data. Asangani and colleagues treated PC3 cells for 24 hours with (+)-JQ1 and dosed at concentration of 500 nmol/L, which did not reduce MYC protein levels by Western blot analysis. In our study, we treated PC3 cells with (+)-JQ1 at a dose of 1 μmol/L for 48 hours, which did reduce MYC mRNA. Our higher dose and longer drug exposure may account for why we observe anti-MYC effects that the previous authors did not report. Importantly, we also show anti-MYC effects in PC3 with a structurally discrete BET bromodomain inhibitor.

MYC hyperactivity in other cancers has also been associated with specific imaging patterns. Palaskas and colleagues reported that ^{18}F-FDG specifically demarcated basal-like breast cancer with MYC hyperactivity (28). It is unclear whether there is a relationship between MYC and ^{18}F-FDG avidity in prostate cancer, particularly given that CRPC is not avid for ^{18}F-FDG in most circumstances.

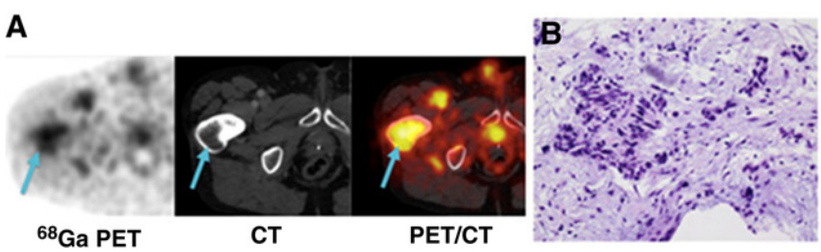

Figure 6.
A, Axial PET, CT, and fused ^{68}Ga-citrate PET/CT showing a ^{68}Ga-citrate–avid lesion within the right femur with no CT correlate (blue arrow).
B, Representative pathology image of the metastasis from the patient's biopsy demonstrating SCNC.

The case examples discussed demonstrate the potential utility of ^{68}Ga-citrate PET as a detection and treatment response monitoring tool for therapies applied against the MYC signaling pathway in SCNC. Given the likely growing prevalence of SCNC as a resistance mechanism to potent androgen signaling blockade, and the lack of validated methods to identify SCNC differentiation other than metastatic tumor biopsy, there is a clear need to develop noninvasive biomarkers to detect and monitor treatment response in this highly aggressive, lethal disease subset. Our studies with ^{68}Ga-citrate come at an opportune time given the recent FDA approval of ^{68}Ga-DOTA-TATE for the detection of neuroendocrine tumors. Preliminary reports with DOTA-TATE imaging in CRPC indicate potential utility of detecting lesions with neuroendocrine differentiation (29). However, the range of uptake is modest, and it is unclear whether DOTA-TATE avidity will be observed in higher grade tumors, analogous to the inverse correlation between tracer uptake and tumor grade observed with neuroendocrine tumors of gastrointestinal origin. Further patient studies with paired ^{68}Ga-citrate PET scan coupled with tumor biopsies to explore the relationship between SCNC differentiation and ^{68}Ga-citrate uptake on PET scan are under way.

Disclosure of Potential Conflicts of Interest

S.C. Behr reports receiving other commercial research support from, has received speakers bureau honoraria from, and is a consultant/advisory board member for GE Healthcare. M.J. Evans reports receiving a commercial research grant from GE Healthcare and is a consultant/advisory board member for ORIC Pharmaceuticals, Inc. No potential conflicts of interest were disclosed by the other authors.

Disclaimer

The content is solely the responsibility of the authors and does not necessarily represent the official views of the NIH.

Authors' Contributions

Conception and design: R. Aggarwal, S.C. Behr, C. Truillet, C.J. Ryan, E.J. Small, M.J. Evans

Development of methodology: R. Aggarwal, S.C. Behr, P.L. Paris, J. Huang

Acquisition of data (provided animals, acquired and managed patients, provided facilities, etc.): R. Aggarwal, S.C. Behr, C. Truillet, M.F.L. Parker, J. Wei, B. Hann, J. Youngren, J. Huang, N. Ranatunga, E. Chang, K.T. Gao, C.J. Ryan, M.J. Evans

Analysis and interpretation of data (e.g., statistical analysis, biostatistics, computational analysis): R. Aggarwal, S.C. Behr, C. Truillet, M.F.L. Parker, L.T. Huynh, J. Wei, C.J. Ryan, M.J. Evans

Writing, review, and/or revision of the manuscript: R. Aggarwal, S.C. Behr, P.L. Paris, L.T. Huynh, E. Chang, E.J. Small, M.J. Evans

Administrative, technical, or material support (i.e., reporting or organizing data, constructing databases): S.C. Behr, J. Wei, J. Youngren, E. Chang, K.T. Gao, M.J. Evans

Study supervision: R. Aggarwal, S.C. Behr, M.J. Evans

Grant Support

This research was supported by a Stand Up To Cancer - Prostate Cancer Foundation Prostate Dream Team Translational Research grant (SU2C-AACR-DT0812, principal investigator: E.J. Small). This research grant was made possible by the generous support of the Movember Foundation. M.J. Evans and R. Aggarwal are Young Investigator Awardees from the Prostate Cancer Foundation. M.J. Evans was supported by the NIH (R00CA172695, R01CA17661), a Department of Defense Idea Development Award (PC140107), the UCSF Academic Senate, and GE Healthcare. C. Truillet was supported by a postdoctoral fellowship from the Department of Defense Prostate Cancer Research Program (PC151060). M.F.L. Parker was supported by a postdoctoral fellowship from the Department of Defense Prostate Cancer Research Program (PC161005). Research from UCSF reported in this publication was supported in part by the NCI of the NIH under award number P30CA082103.

The costs of publication of this article were defrayed in part by the payment of page charges. This article must therefore be hereby marked *advertisement* in accordance with 18 U.S.C. Section 1734 solely to indicate this fact.

Received April 12, 2017; revised May 17, 2017; accepted June 2, 2017; published OnlineFirst June 7, 2017.

References

1. Ellwood-Yen K, Graeber TG, Wongvipat J, Iruela-Arispe ML, Zhang J, Matusik R, et al. Myc-driven murine prostate cancer shares molecular features with human prostate tumors. Cancer Cell 2003;4:223–38.
2. Cho H, Herzka T, Zheng W, Qi J, Wilkinson JE, Bradner JE, et al. RapidCaP, a novel GEM model for metastatic prostate cancer analysis and therapy, reveals myc as a driver of Pten-mutant metastasis. Cancer Discov 2014; 4:318–33.
3. Koh CM, Bieberich CJ, Dang CV, Nelson WG, Yegnasubramanian S, De Marzo AM. MYC and prostate cancer. Genes Cancer 2010;1:617–28.
4. Beltran H, Rickman DS, Park K, Chae SS, Sboner A, MacDonald TY, et al. Molecular characterization of neuroendocrine prostate cancer and identification of new drug targets. Cancer Discov 2011;1:487–95.
5. Aparicio A, Tzelepi V. Neuroendocrine (small-cell) carcinomas: why they teach us essential lessons about prostate cancer. Oncology 2014;28:831–8.
6. Lee JK, Phillips JW, Smith BA, Park JW, Stoyanova T, McCaffrey EF, et al. N-Myc drives neuroendocrine prostate cancer initiated from human prostate epithelial cells. Cancer Cell 2016;29:536–47.
7. Asangani IA, Wilder-Romans K, Dommeti VL, Krishnamurthy PM, Apel IJ, Escara-Wilke J, et al. BET bromodomain inhibitors enhance efficacy and disrupt resistance to AR antagonists in the treatment of prostate cancer. Mol Cancer Res 2016;14:324–31.
8. Asangani IA, Dommeti VL, Wang X, Malik R, Cieslik M, Yang R, et al. Therapeutic targeting of BET bromodomain proteins in castration-resistant prostate cancer. Nature 2014;510:278–82.
9. Wyce A, Degenhardt Y, Bai Y, Le B, Korenchuk S, Crouthame MC, et al. Inhibition of BET bromodomain proteins as a therapeutic approach in prostate cancer. Oncotarget 2013;4:2419–29.
10. Stice JP, Wardell SE, Norris JD, Yllanes AP, Alley HM, Haney VO, et al. CDK4/6 therapeutic intervention and viable alternative to taxanes in CRPC. Mol Cancer Res 2017;15:660–9.
11. Kirschner AN, Wang J, van der Meer R, Anderson PD, Franco-Coronel OE, Kushner MH, et al. PIM kinase inhibitor AZD1208 for treatment of MYC-driven prostate cancer. J Nat Cancer Inst 2014;107:pii: dju407.
12. Pandit-Taskar N, Veach DR, Fox JJ, Scher HI, Morris MJ, Larson SM. Evaluation of castration-resistant prostate cancer with androgen receptor-axis imaging. J Nucl Med 2016;57:73S–8S.
13. Bambury RM, Scher HI. Enzalutamide: development from bench to bedside. Urol Oncol 2015;33:280–8.
14. O'Donnell KA, Yu D, Zeller KI, Kim JW, Racke F, Thomas-Tikhonenko A, et al. Activation of transferrin receptor 1 by c-Myc enhances cellular proliferation and tumorigenesis. Mol Cell Biol 2006;26:2373–86.
15. Huang CH, Lujambio A, Zuber J, Tschaharganeh DF, Doran MG, Evans MJ, et al. CDK9-mediated transcription elongation is required for MYC addiction in hepatocellular carcinoma. Genes Dev 2014;28: 1800–14.
16. Holland JP, Evans MJ, Rice SL, Wongvipat J, Sawyers CL, Lewis JS. Annotating MYC status with 89Zr-transferrin imaging. Nat Med 2012; 18:1586–91.
17. Doran MG, Carnazza KE, Steckler JM, Spratt DE, Truillet C, Wongvipat J, et al. Applying Zr-transferrin to study the pharmacology of inhibitors to BET bromodomain containing proteins. Mol Pharm 2016;13: 683–8.

18. Evans MJ. Measuring oncogenic signaling pathways in cancer with PET: an emerging paradigm from studies in castration-resistant prostate cancer. Cancer Discov 2012;2:985–94.
19. Larson SM, Rasey JS, Allen DR, Nelson NJ, Grunbaum Z, Harp GD, et al. Common pathway for tumor cell uptake of gallium-67 and iron-59 via a transferrin receptor. J Nat Cancer Inst 1980;64:41–53.
20. Behr SC, Aggarwal R, Seo Y, Aparici CM, Chang E, Gao KT, et al. A feasibility study showing [Ga]Citrate PET detects prostate cancer. Mol Imaging Biol 2016;18:946–51.
21. Scher HI, Halabi S, Tannock I, Morris M, Sternberg CN, Carducci MA, et al. Design and end points of clinical trials for patients with progressive prostate cancer and castrate levels of testosterone: recommendations of the prostate cancer clinical trials working group. J Clin Oncol 2008;26:1148–59.
22. Sun Y, Niu J, Huang J. Neuroendocrine differentiation in prostate cancer. Am J Translat Res 2009;1:148–62.
23. Truillet C, Cunningham JT, Parker MF, Huynh LT, Conn CS, Ruggero D, et al. Non-invasive measurement of mTORC1 signaling with 89Zr-transferrin. Clin Cancer Res 2017;12:3045–52.
24. Evans MJ, Holland JP, Rice SL, Doran MG, Cheal SM, Campos C, et al. Imaging tumor burden in the brain with 89Zr-transferrin. J Nucl Med 2013;54:90–5.
25. Kumar V, Boddeti DK, Evans SG, Angelides S. (68)Ga-Citrate-PET for diagnostic imaging of infection in rats and for intra-abdominal infection in a patient. Curr Radiopharm 2012;5:71–5.
26. Taylor BS, Schultz N, Hieronymus H, Gopalan A, Xiao Y, Carver BS, et al. Integrative genomic profiling of human prostate cancer. Cancer Cell 2010; 18:11–22.
27. Robinson D, Van Allen EM, Wu YM, Schultz N, Lonigro RJ, Mosquera JM, et al. Integrative clinical genomics of advanced prostate cancer. Cell 2015;161:1215–28.
28. Beltran H, Prandi D, Mosquera JM, Benelli M, Puca L, Cyrta J, et al. Divergent clonal evolution of castration-resistant neuroendocrine prostate cancer. Nat Med 2016;22:298–305.
29. Hope TA, Aggarwal R, Simko JP, VanBrocklin HF, Ryan CJ. Somatostatin imaging of neuroendocrine-differentiated prostate cancer. Clin Nucl Med 2015;40:540–1.